

Accepted Manuscript

Title: Selective hydrogenation of aromatic carboxylic acids over basic N-doped mesoporous carbon supported palladium catalysts

Author: Hezhan Jiang Xiaolong Yu Renfeng Nie Xinhuan Lu
Dan Zhou Qinghua Xia



PII: S0926-860X(16)30179-X
DOI: <http://dx.doi.org/doi:10.1016/j.apcata.2016.04.009>
Reference: APCATA 15837

To appear in: *Applied Catalysis A: General*

Received date: 25-1-2016
Revised date: 8-4-2016
Accepted date: 11-4-2016

Please cite this article as: Hezhan Jiang, Xiaolong Yu, Renfeng Nie, Xinhuan Lu, Dan Zhou, Qinghua Xia, Selective hydrogenation of aromatic carboxylic acids over basic N-doped mesoporous carbon supported palladium catalysts, *Applied Catalysis A, General* <http://dx.doi.org/10.1016/j.apcata.2016.04.009>

This is a PDF file of an unedited manuscript that has been accepted for publication. As a service to our customers we are providing this early version of the manuscript. The manuscript will undergo copyediting, typesetting, and review of the resulting proof before it is published in its final form. Please note that during the production process errors may be discovered which could affect the content, and all legal disclaimers that apply to the journal pertain.

Submitted to *Applied Catalysis A: General* for publication

Title:

Selective hydrogenation of aromatic carboxylic acids over basic N-doped mesoporous carbon supported palladium catalysts

Authors:

Hezhan Jiang, Xiaolong Yu, Renfeng Nie^{*}, Xinhuan Lu, Dan Zhou, Qinghua Xia^{*}

Address:

Hubei Collaborative Innovation Center for Advanced Organic Chemical Materials, & Ministry-of-Education Key Laboratory for the Synthesis and Application of Organic Functional Molecules, School of Chemistry and Chemical Engineering, Hubei University, Wuhan 430062, P.R. China

* Corresponding author

Renfeng Nie, Hubei University, Wuhan 430062, P.R. China

Tel/Fax: 86-27-88662747

Email: refinenie@163.com

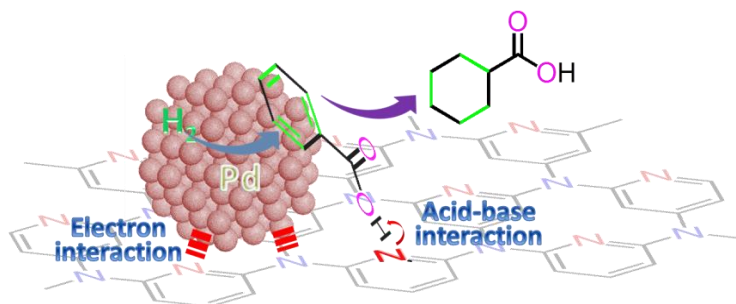
Qinghua Xia, Hubei University, Wuhan 430062, P.R. China

Tel/Fax: 86-27-88662747

Email: xiaqh518@aliyun.com

Hubei Collaborative Innovation Center for Advanced Organic Chemical Materials, & Ministry-of-Education Key Laboratory for the Synthesis and Application of Organic Functional Molecules, School of Chemistry and Chemical Engineering, Hubei University, Wuhan 430062, P.R. China

Graphic abstract



Pd NPs are supported on MCN that is prepared *via* polymerization between ethylenediamine and carbon tetrachloride. The negative charge and the basicity on MCN surface are originated from its rich carbon nitride heterocycles. The negative charge contributes to strong N-Pd interaction and the basicity generates higher adsorption capacity for acid substrates, both of which may lead to its high activity for selective ring hydrogenation of aromatic compounds.

Highlights:

- Pd NPs are supported on MCN that is prepared via polymerization between ethylenediamine and carbon tetrachloride.
- N-Pd interaction affords high dispersion and durability of Pd NPs.
- MCN shows higher adsorption capacity for acid substrates than AC and NAC.
- High N content (18.5 wt %) leads to negative charge of MCN and much higher activity in water.
- Pd/MCN shows better performance for hydrogenation of acidic compounds than Pd/AC and Pd/NAC.

Abstract

Mesoporous carbon nitride (MCN) has been prepared through a simple polymerization reaction between ethylenediamine (EDA) and carbon tetrachloride (CTC) by a nano hard-templating approach. The obtained MCN possesses high surface area (166.3 m²/g), average pore size of 9.2 nm and high N content (up to 18.5 wt %). The negative charge and the basicity on MCN surface are originated from its rich carbon nitride heterocycles, which notably improves the surface hydrophilicity and the adsorption of acidic molecules. Furthermore, MCN can be adopted as the proper support for highly dispersed Pd NPs with well-controlled size distribution.

Compared with microporous N-doped active carbon with low N-content, the MCN-supported Pd catalyst shows an enhanced activity in water phase for the selective ring hydrogenation of benzoic acid, benzamide and phenol, in which 11.3 times higher activity in comparison to undoped catalyst is achieved. Wide characterizations reveal that big pore size, selective adsorption for acid substrate and strong interaction between N and Pd may lead to the high activity of Pd/MCN.

Keywords: Mesoporous carbon nitride; polymerization; basicity; palladium; selective hydrogenation.

1. Introduction

Catalytic reduction on nanoparticle surfaces is one of the most important reactions for the conversion of raw materials and the production of chemicals [1, 2]. The development of new materials holds the key to fundamental advances in catalysis, further meeting the environmentally-benign and energy-saving requirements [3]. The transformation of aromatics into value-added chemicals or high-quality fuels is an important class of reactions [4, 5]. For example, the ring hydrogenation of benzoic acid (BA) is the most effective method in the synthesis of cyclohexane carboxylic acid (CCA), which is an important organic intermediate for the synthesis of pharmaceuticals like praziquantel and ansatrienin [6]. Usually, the hydrogenation of aromatic ring with electron-withdrawing groups requires more severe conditions than that with electron-donating groups [7], which will result in the occurrence of some undesired side reactions, such as the hydrogenation of carboxylic groups into alcohols at high temperature/pressure [8]. Thus, there is a need for the design of the catalyst with high activity and stability based on economic and environmental considerations.

In terms of industrial applications, the use of heterogeneous catalysts instead of homogeneous ones is preferred due to the easy of their separation and recycling.

Metal NPs, prepared from metal salts with stabilizers and supported on metal oxides, carbon or zeolites, are attractive for catalysis because of large surface area-to-volume ratio and effective use of metals [9, 10]. In addition, the variation of nanoparticle size sometimes allows a control over the activity when catalytic reactions occur on the surface of NPs [10]. However, the decrease in the activity of immobilized catalysts is frequently observed, possibly assigned to metal leaching or aggregation of NPs because of the weak interaction between active ingredients and support surface [11, 12]. Therefore, attempts to control the dispersion and the catalytic durability of metal NPs are essential, for which one approach to enhance the dispersion and stability of NPs lies in the use of the pore-rich supports. For example, Pd species can be encapsulated in pores of microporous and mesoporous materials (zeolites, MOFs, carbon, etc.) due to their confinement effects [7, 13-15], but low catalytic activity is sometimes caused by the mass diffusion resistance [16, 17]. Though the heterogenization of the existing homogeneous palladium catalysts immobilized on the surface of polymers and silica is another method to prepare highly dispersed metal catalysts [18-20], the reaction scope is limited and the leaching or decomposition may cause irreversible deactivation under harsh conditions. Moreover, the addition of the second components (metal or metal oxide) as building blocks for mediating the particle size and stability of NPs at multiple junction points is also reported [21-24].

Nitrogen-containing carbons, as a kind of fascinating materials, have attracted worldwide attention recently [25]. It has been reported that N-dopants in the carbon skeleton can be inbuilt on the surface, which can provide a platform for the grafting of metal NPs, leading to the carbon-based catalysts with well-dispersed catalytic active sites [26, 27]. At the same time, the N doping results in an improvement in the hydrophilicity and basicity of supports [11], beneficial to the use of as-prepared catalysts in aqueous phase and the selective adsorption of acidic molecules through the acid–base interaction [28]. The introduction of N can modify the electronic structure of carbon matrix, and strengthen the interaction between carbon and guest molecules due to the high charge and spin density caused by the nitrogen [29], which

can simultaneously tune the activity of the sp^2 carbon in the H_2 activation by lowering down its dissociation energy, thus promoting the catalytic hydrogenation [30]. To date, many studies have reported the improved catalytic activity of carbon-based catalysts by increasing the metal dispersion initiated by N-doping [12, 31-33]. Moreover, the presence of N-dopants on the carbon skeleton could also modify the electronic and chemical interactions with the deposited active phase to greatly enhance the overall catalytic activity and selectivity as well [34, 35].

Up to now, although various catalysts, including carbon-supported precious metals (Pd/CN, Ru/C) [36, 37] and metal alloys (Pd-Ru [38], RuPt [39], Ni-Zr-B [40, 41]), have been studied in the selective hydrogenation of benzoic acid (BA), it is still one big challenge to overcome the high resonance energy of aromatic ring [42]. Herein, the investigations on N-containing carbon (including microporous N-doped active carbon (NAC) and mesoporous carbon nitride (MCN)) serving as basic supports to achieve highly dispersed Pd NPs are reported. These N-doping materials show high activity for the selective hydrogenation of aromatic ring in water phase.

2. Experimental section

2.1. Catalyst Preparation

Active carbon (AR) was purchased from Hunan Xiangda Chemical Reagent Co.. Fumed silica (SiO_2) with the surface area of $250\text{ m}^2/\text{g}$ was obtained from Degussa Co. (Germany). Dicyandiamide (CP, 98 %), ethylenediamine (AR), carbon tetrachloride (AR), benzoic acid (AR, 99.5 %), H_2O_2 (28 %), $PdCl_2$ (AR, Pd >59 %), and other chemicals (analytical grade) were purchased from Aladdin Chemicals and used as received without further purification. The phenol was purchased from Sinopharm Chemicals in China.

2.2. Preparation of N-doped carbon

N-doped active carbon (NAC) was synthesized *via* a heat treatment of the mixture consisted of dicyandiamide as the nitrogen source and commercial active carbon as the precursor. Typically, ten grams of active carbon (AC) was first

immersed in 250 mL H₂O₂ (28 wt %) solution. The slurry was stirred and treated at 50 °C for 5 h. Then the solid was recovered by filtration and washed thoroughly with DI water. Thus-pretreated AC was dried in a vacuum oven at 80 °C for 10 h, which was denoted as H₂O₂-AC. One half gram of dicyandiamide was added into a suspension of 2.0 g H₂O₂-AC in 100 mL DI water while stirring. The slurry was stirred for 30 min at 60 °C and sonicated for 30 min (200 W, 50 Hz), and then water was removed by reduced pressure at 60 °C. The resulting powder was transferred into a crucible, heated to 600 °C at a rate of 2 °C·min⁻¹ under a flow of nitrogen and kept for 4 h. The sample was then cooled down to room temperature under the protection of N₂. The carbon material was denoted as NAC.

MCN was synthesized by hard template method. Typically, 0.5 g fumed silica was dispersed into a mixed solution of ethylenediamine (EDA, 5.4 g) and tetrachloromethane (CTC, 12 g) under stirring. The above mixture was heated at 90 °C for 6 h and then dried in an oven for 12 h. The templated-carbon nitride polymer composite was heated to 600 °C at a heating rate of 3 °C·min⁻¹ under a flow of nitrogen and kept for 5 h. The carbonized material was treated with 5 wt % hydrofluoric acid. The solid was recovered by filtration, washed with ethanol and dried at 100 °C. The resultant sample was denoted as MCN.

2.3 Preparation of Pd NPs over N-doped carbon

One gram of the support (NAC or MCN) was dispersed in DI water (50 mL), then added with 41.7 mg PdCl₂ (2.5 wt %) while stirring. After 30 min, the reduction treatment was performed in a 100 mL Teflon-lined autoclave at 40 °C for 8 h under 2 MPa H₂. Then, the precipitate was recovered by filtration and washed thoroughly with DI water. The resulting Pd catalyst was dried in an oven at 80 °C overnight and named as Pd/NAC or Pd/MCN. The synthesis of Pd/AC was the same as that of Pd/NAC, in which AC was pretreated at 600 °C for 4 h under N₂ protection. MgO-, Al₂O₃-, and SiO₂-supported Pd catalysts (with 2.5 % loading amount of Pd) were also synthesized by the method similar to that for Pd/NAC, which were then used in the reactions without further treatment. The real loading

amount of Pd was detected *via* an ICP analysis.

2.4 Characterization

Powder X-ray diffraction (XRD) was performed on a Bruker D8A25 diffractometer with $\text{CuK}\alpha$ radiation ($\lambda = 1.54184 \text{ \AA}$) operating at 30 kV and 25 mA. For the detection of FTIR spectra, a mixture of 3 mg catalyst powder and 200 mg KBr was pressed into a thin wafer. Raman spectra were collected at room temperature from 100 to 4000 cm^{-1} with 514.5-nm argon ion laser (Rhenishaw Instruments, England). The spectra were recorded at a resolution of 2 cm^{-1} . N_2 adsorption was carried out at $-196 \text{ }^\circ\text{C}$ using an auto-adsorption analyzer (Micromeritics, TriStar II). Zeta potential was measured with 12.5 mg of samples dispersed in 25 mL buffer solution ($\text{pH} = 7.00 \pm 0.02$) on a zeta potential analyzer BIC PALS. The elemental analysis for the content of non-metallic elements was performed using a vario EL III Elementar. The ICP analysis was conducted by inductively coupled plasma-atomic emission spectroscopy (Plasma-Spec-II spectrometer). Scanning electron images (SEM) were collected on JEOL (JSM6700F) at an accelerating voltage of 15 kV. Transmission electron microscope (TEM) images were obtained using an accelerating voltage of 200 kV on a JEOL-135 2010F Transmission Electron Microscope. X-ray photoelectron spectra (XPS) were recorded on a Perkin-Elmer PHI ESCA system. X-ray source was standard Mg anode (1253.6 eV) at 12 kV and 300 W.

2.5 Adsorption isotherms for benzoic acid

In a typical process, 20 mg AC, NAC or MCN was added into 50 mL aqueous solution of benzoic acid (200 ppm), and the adsorption was performed at $25 \text{ }^\circ\text{C}$ in a water bath with magnetic stirring (stirring rate: 1,000 r.p.m.). After completion of the adsorption, the solid catalyst was separated by centrifugation and the liquid phase was analyzed by GC.

2.6 Catalytic tests

The hydrogenation reactions were carried out in a 25 mL stainless autoclave

with a Teflon liner. In a typical run, 20 mg catalyst and 61 mg (0.5 mmol) benzoic acid was dispersed in 5 mL DI water. The autoclave was sealed, purged and pressurized with hydrogen to 2.5 MPa, and then heated to 110 °C under magnetic stirring at a rate of 1000 rpm. After the completion of the reaction, the mixture was extracted by ethyl acetate and centrifuged in order to remove the solid catalyst. The solid catalyst was recovered by centrifugation and washed sequentially with ethyl acetate, ethanol and DI water. The filtrate was analyzed by gas-chromatograph (GC, HP 5890, USA) equipped with a 30 m capillary column (HP-5) and a flame ionization detector (FID). All the products were confirmed by GC–MS (Agilent 6890).

3. Results and discussion

3.1. Structural characterizations

SEM images (Fig. 1) show flake-like morphology of pristine AC and NAC, different from an irregular morphology of MCN with some loose pore structures originated from the removal of template. Type I isotherms are observed from nitrogen sorption analysis of AC and NAC (Fig. 2), indicative of the nature of microporous structure [43]. Compared with AC, N-doping leads to slight decreases in BET area and pore volume for NAC, indicating the partial occupation/blockage of the pore channels of AC by N dopants. MCN shows a H₄ hysteresis loop on the isotherm and a sharp rise at relative pressure higher than 0.60, characteristic of textural mesopores [44]. The average pore size of AC, NAC or MCN is calculated to be 4.3, 4.1 or 9.2 nm, respectively. Moreover, MCN shows S_{total} area of 166.3 m²/g and pore volume of 0.33 cm³/g (Table 1), dominated with mesopores in a proportion of around 81.8 %, much higher than 45.5 % of AC and 40.0 % of NAC.

The FT-IR spectra are shown in Fig. S1, where contains two bands at 1207 and 1630 cm⁻¹ ascribed to aromatic C–N and C=N stretching bonds, respectively [44]. Clearly those bands for MCN seem to be strengthened in comparison to NAC, indicating the existence of more rich N groups on the surface of MCN.

The chemical compositions of N-doped carbon materials are determined by CHNS

elemental analysis and XPS spectra (Table 2). The surface N content of NAC obtained from the XPS data is 3.76 %, significantly higher than the bulk nitrogen content (2.35 %) detected by elemental analysis, indicating that the N species are more enriched on the surface than in the bulk. However, the nitrogen content of MCN is 18.5 %, which is homogeneously distributed in MCN.

The Raman spectra are shown in Fig. S2, the G band at $\sim 1590 \text{ cm}^{-1}$ is attributed to the in-plane vibration of sp^2 carbon atoms, while the D band at $\sim 1350 \text{ cm}^{-1}$ is a defect-induced Raman feature representing the imperfect crystalline structure [45]. Compared with the AC, the NAC shows an increased I_D/I_G value (1.13), indicating the formation of more structural defects in carbon skeleton. As for the MCN, the G band is obviously stronger than the D band ($I_D/I_G = 0.88$), accompanied with a shift of the G band position to a low frequency (1569 cm^{-1}), indicating that sp^2 hybridized carbon and nitrogen atoms are distributed throughout the graphitized layers [44].

The main C1s peak of N-doped carbon (Fig. 3a) locates at approximately 284.5 eV with a tail peak at high binding energy of around 285.8 eV, assigned to the electron-deficient carbons bound to nitrogen (C=N or C-N) [46, 47]. For MCN, the C=N/C-N signals are significantly strengthened, suggesting that more N species have been incorporated into the skeleton of carbon, well agreed with the element analysis.

The N1s spectra (Fig. 3b) of NAC and MCN are broad and asymmetric. The curve deconvolution shows that the N1s spectra can be well-fitted to the superposition of four peaks centered at 398.5, 400.1, 401.1, and 403.3 eV, which are attributed to aromatic/pyridinic nitrogen (N1), sp^2 -hybridized/pyrrolic nitrogen (N2), sp^3 -hybridized terminal/quaternary nitrogen (N3), and pyridine oxide-N (N4), respectively [48, 49]. The contents of four types of nitrogen atoms are listed in Table 3. N1 and N2 species in NAC are dominant nitrogen-containing surface functional groups, with a total content of 91.2 %. Comparatively, the content of N1 and N2 in MCN is 66.5 %, along with a N3 content of 31.7 %. These N1 and N2 species can act as basic sites on the carbon surface [28], and N1, N2 and N3 can add the electron density at the doped sites to act as a coordinative site of metal ions and as a defect site for the enhanced interaction among polarized molecules [29, 31, 34, 50]. As shown in

Table 1, the zeta potentials of AC, NAC and MCN dispersed in DI water are measured to be -0.02, -17.0 and -25.4 mV, respectively. The lower zeta potentials of NAC and MCN with more negatively charged surface may be explained by the presence of rich nitrogen dopants (especially for N1 and N2) on the surface [34]. Meanwhile, the lower zeta potential means the higher surface basicity that will require more protons to neutralize [51].

In order to characterize the Pd NPs on carbon surface, XRD, TEM and XPS have been carried out. The XRD patterns of Pd/AC, Pd/NAC and Pd/MCN are shown in Fig. 4. The diffraction peaks at 40.0° and 46.5° are indexed to the (111) and (200) planes in the face centered cubic (FCC) crystal structure of Pd [52]. Upon the N-incorporation in carbon, the intensity of Pd diffraction peaks in Pd/NAC and Pd/MCN decreases and becomes faint, indicating the decrease of Pd crystalline size. According to Scherrer's formula and the half-width of (111) peak, the calculated sizes of Pd crystallites in Pd/NAC and Pd/MCN are 2.4 and 3.8 nm (Table 3), respectively, notably smaller than 10.8 nm of Pd/AC.

The Pd dispersion on carbon supports have been further confirmed by TEM observations in Fig. 5. It is found that the particle size of Pd NPs on the surface of AC ranges from 6 to 18 nm. While the uniformly well-dispersed Pd NPs on very large surfaces of MCN and NAC can be observed, without any aggregation of NPs into large clusters. A high-resolution TEM image of Pd/MCN clearly shows that the distance between two adjacent lattice planes of Pd NPs is approximately 0.226 nm. In addition, the average Pd sizes with standard deviation in Pd/AC, Pd/NAC and Pd/MCN are 12.0 ± 2.5 , 3.1 ± 0.7 and 4.3 ± 1.2 nm, respectively.

N-incorporation changes the surface functional groups, accompanied with increasing the surface hydrophilicity and surface negatively-charged sites (Table 1). The improved hydrophilicity favors its dispersion in polar solvents (such as water), and the negatively-charged surface facilitates the electrostatic attraction of the positively charged metallic ions as well as the hydrolysis of Pd^{2+} ions for its immobilization onto the support. In addition, the micropore of NAC may further

improve the Pd dispersion by its confinement effects [53]. All these factors facilitate the formation of evenly dispersed Pd NPs on N-doped support.

The Pd⁰ 3d_{5/2} and 3d_{3/2} doublets are observed at 335.6 and 340.9 eV, as shown in Fig. 6. Palladium in the oxidation state is also detected (doublet pair at 337.7 and 342.9 eV). The presence of Pd^{δ+} species, characterizing both the deposition of pure and N-doped carbon, can be attributed to the oxidation of Pd due to the formation of Pd-O bond by air exposure. As shown in Table 3, the percentages of Pd^{δ+} on NAC (84.5 %) and MCN (53.9 %) are much higher than that of N-free AC (21.4 %). As we know, the oxygen groups on support surfaces facilitate the anchoring of metal NPs [51], and the oxygen content on all supports is similar (Table 2), indicating the important role of N dopant on influencing the electronic properties of Pd. Previous results in the literature suggested that pyridinic N and quaternary-N sites could facilitate both the coordination of metal ions and the anchoring of metal NPs. [50]. XPS spectra show that pyridinic or aromatic (C=N-C) nitrogen atoms exist prevalently in N-doped carbons, which are often associated with defect sites on edges of graphite layers or on vacancy sites [54, 55]. At the same time, Li et al. [56] showed that the interaction of Pt with the carbon system containing quaternary N atoms was weaker than that with the carbon system containing pyridinic N atoms on vacancy sites. It is reported that the divalent Pd species are more abundant when Lewis basic sites in the form of pyridine N species are present, which indicates that the coordination at these sites lowers down their reducibility at the reduction conditions used [34]. These results indicate that pyridinic or pyrrolic nitrogen atoms can interact intensively with Pd, thus leading to the high percentage of Pd^{δ+} species.

The strong interaction between support and Pd can be evidenced by H₂-TPR measurement compared with that of Pd/AC (Fig. 7). In the curve of Pd/AC, a hydrogen release peak at around 60 °C may be attributed to desorption of hydrogen pre-absorbed by Pd NPs [38]. The broad reduction peak centered at 139 °C can be ascribed to the reduction of Pd^{δ+} to Pd⁰. However, the reduction curves of Pd/NAC and Pd/MCN show two hydrogen consumption peaks with maximum at about 195 and 280 °C, indicating the formation of two types of Pd on support. The higher reduction

temperature indicates the stronger interaction between support and Pd. These peaks may be related to Pd species that strongly interact with aromatic N (pyridinic and pyrrolic N) groups [34]. The π -bonded planar C-N-C structures, along with the unsaturated nitrogen groups at the edges of the support, are suitable sites for anchoring Pd species, where strong metal-support interactions may take place [57]. The strong coordination of Pd species at N sites may be beneficial for high dispersion and stability of Pd NPs on support.

3.2. Catalytic activity for the hydrogenation of aromatic ring

The hydrogenation of BA to CCA is carried out at 110 °C under 2.5 MPa (Table 4). In blank test, when no catalyst is used, no BA is transformed (entry 1). Obviously, N-free catalyst (Pd/AC, entry 2) shows a poor activity with 7.2 % conversion in this transformation. By comparison, all N-doped catalysts (entries 3-5) exhibit significantly higher catalytic activity. For example, Pd/NAC affords 48.2 % BA conversion. As for Pd/MCN, the BA conversion reaches as high as 81.5 %, a further prolongation of reaction time to 2.5 h leads to a full conversion of BA with 100% CCA selectivity (entry 5). Other frequently used heterogeneous Pd-based catalysts inclusive of Pd/SiO₂, Pd/Al₂O₃, Pd/MgO and commercial Pd/AC (entries 6-9) achieve a poor hydrogenation activity < 25 % under the same reaction conditions.

It must be noted that the solvent plays a key role in determining the reaction rate or the distribution of products. Among these solvents tested (Fig. 8), both apolar and protic organic solvents are unfavourable for the titled reaction on Pd/MCN, giving a low hydrogenation activity < 2 %. Although water has the lowest solubility of H₂ than other solvents [36], it results in the highest conversion of 81.5 % for Pd/MCN, which can be ascribed to strong H-bond donor capability of water [58].

Although Pd/NAC processes higher Pd dispersion, it offers lower catalytic activity in comparison to Pd/MCN, indicative of the crucial role of mesoporous structure (a mesopore proportion of 81.8 %) for substrate diffusion and hydrogenation on Pd NPs. What's more, considering the rich basic sites of N-doped support, the adsorption capacity of BA on AC, NAC or MCN is measured. As shown in Fig. 9, the adsorption

capacity of BA over MCN (228 mg/g) is larger than that of AC (92 mg/g) and NAC (131 mg/g), exhibiting a favorable interaction between an acid (BA) and base (MCN). The strong adsorption leads to an increased BA concentration and accelerated reaction rate on surface of Pd/MCN.

The Pd/MCN catalyst can be easily recovered and reused for five times without significant loss of efficiency (Fig. 10), and the ICP analysis of fresh and recovered catalysts reveals negligible Pd leaching (< 0.05 ppm) in solution. The crystalline state and dispersion of Pd NPs in recovered Pd/MCN, based on the corresponding XRD pattern (Fig. S3) and TEM image (Fig. S4), do not change significantly after five runs. The XPS analysis of recovered Pd/MCN shows a higher Pd⁰ ratio (57.7 %) than that of fresh catalyst (Fig. S5), indicative of partial reduction of Pd^{δ+} during the hydrogenation reaction.

The difference in activity between the catalysts becomes more conspicuous through the hydrogenation of more sensitive benzamide in water (Table 5). Pd/AC, Pd/NAC and Pd/MCN afford 4.4, 15.5 and 55.6 % benzamide conversion at 85 °C for 8 h. Moreover, higher temperature (110 °C) leads to fast hydrogenation rate but decreased product selectivity (91 %) due to the hydrolysis of amide bond. Because of the great importance of cyclohexanone [59], the selective hydrogenation of phenol is carried out further. Previous study finds that the phenol hydrogenation is a structural sensitive reaction [60]. For example, phenol adsorbed in nonplanar fashion over basic sites gives rise to cyclohexanone while that adsorbed on acidic sites in coplanar fashion leads to the formation of cyclohexanol and cyclohexane [61, 62]. Therefore, the selective hydrogenation of acidic phenol is performed over basic Pd/MCN catalyst under a mild condition (40 °C, 0.3 MPa H₂) (Table 6). Using N-free AC as support gives only 24.8 % phenol conversion and 93.5 % cyclohexanone selectivity (entry 1). Comparatively, Pd/NAC (entry 2) gives an improved conversion (53.7 %) and selectivity (95.1 %). The phenol conversion increases quickly to 100 % over Pd/MCN (entry 3) along with a high cyclohexanone selectivity (98.1%).

Using MCN as support, the Pd catalysts with different Pd content are prepared and investigated for BA hydrogenation (Fig. S6). The catalytic activity quickly reaches

from 37.7 % to 81.5 % after 2 h when Pd loading increases from 0.43 to 2.36 wt %. However, a limited increase of the activity occurs when the metal loading is further increased to 4.78 wt %. Moreover, the TOF exhibits a reverse variation trend with increasing loading from 0.43 wt % to 4.78 wt % and the maximum value of 116.2 h^{-1} is achieved over 0.43%Pd/MCN, this value is comparable to those Pd catalysts in water [36], in which the TOF is 106 h^{-1} at $120 \text{ }^\circ\text{C}$ and 4 MPa H_2 .

Clearly, the introduction of N dopant and mesopores is the key to enhance catalytic activity. Firstly, the surface pyridinic or aromatic (C=N-C) nitrogen species provide the co-interaction sites for Pd species, which gives rise to strong metal-N bond at the interface [34], accompanied with well-dispersed Pd NPs. Those small particles are responsible for the enhanced catalytic performance. Moreover, the dominant pyridinic or aromatic (C=N-C) nitrogen can serve as Lewis basic sites to increase the hydrophilicity and basicity of MCN [49], which is beneficial for the dispersion of catalyst in water and adsorption of acid substrates (e.g., benzoic acid, phenol). Third, the high accessibility of active phase derived from the mesoporous structure decreases the mass diffusion resistance in reaction medium, thus accelerating the transformation of substrate.

To further demonstrate the versatility of Pd/MCN, selective hydrogenation of different aromatic acids is investigated (Table 7). *Para*-methylbenzoic acid contains an electron-donating group on the aromatic ring of benzoic acid, which affords a fast hydrogenation rate than benzoic acid (entry 2), giving 98 % conversion in 2 h. Phenylacetic acid (entry 3) shows a slow hydrogenation rate and needs 4 h to give a full transformation. Furthermore, full conversion of methyl benzoate (entry 4) is obtained over Pd/MCN in 6 h. For dimethyl phthalate (DMP, entry 6), a common plasticizer, the conversion is 92 % at 8 h, much slower than that of non-substituted benzoic acid.

4. Conclusion

MCN with high N content (18.5 wt %) is synthesized by nanocasting approach via a simple polymerization reaction between EDA and CTC, and is especially employed

for anchoring well-dispersed Pd NPs under a surfactant-free one-step approach. For selective ring hydrogenation of BA, the resulting Pd/MCN shows 1.7 and 11.3 times activity of microporous N-doped AC and AC-supported catalysts, respectively, and affords high TOF up to 116.2 h⁻¹. This catalyst is stable and active for the hydrogenation of benzamide, phenol and a series of electron-deficient benzoic acids. Wide characterizations disclose that big pore size, rich basic sites on the surface of MCN and intimate interaction between Pd and N lead to the enhanced activity of Pd/MCN in water.

Acknowledgements

This work was supported by National Natural Science Foundation of China (21173073, 21273064), Natural Science Fund for Creative Research Groups of Hubei Province (2014CFA015), Natural Science Fund of Hubei Province (2015CF232), the Key Project of the Education Department of Hubei Province (D20141004), and the 2014 Sci-tech Support Project of the Science and Technology Department of Hubei Province (2014BAA098).

References

- [1] S. Nishimura, Wiley, New York, (2001) 589-590.
- [2] M.I. Bartók, Chem. Rev. 110 (2009) 1663-1705.
- [3] A.S. Arico, P. Bruce, B. Scrosati, J.-M. Tarascon, W. Van Schalkwijk, Nat. mater. 4 (2005) 366-377.
- [4] D. Bianchi, R. Bortolo, R. Tassinari, M. Ricci, R. Vignola, Angew. Chem. Int. Ed. 39 (2000) 4321-4323.
- [5] A. Stanislaus, B.H. Cooper, Catal. Rev. 36 (1994) 75-123.
- [6] B.S. Moore, H. Cho, R. Casati, E. Kennedy, K.A. Reynolds, U. Mocek, J.M. Beale, H.G. Floss, J. Am. Chem. Soc. 115 (1993) 5254-5266.
- [7] P. Zhang, T. Wu, M. Hou, J. Ma, H. Liu, T. Jiang, W. Wang, C. Wu, B. Han, ChemCatChem, (2014) 6 (12)3323-3327.

- [8] E.J. Grootendorst, R. Pestman, R.M. Koster, V. Ponec, Selective Reduction of Acetic Acid to Acetaldehyde on Iron Oxides, *J. Catal.* 148 (1994) 261-269.
- [9] S.F.J. Hackett, R.M. Brydson, M.H. Gass, I. Harvey, A.D. Newman, K. Wilson, A.F. Lee, *Angew. Chem. Int. Ed.* 46 (2007) 8593-8596.
- [10] S. Kidambi, J. Dai, J. Li, M.L. Bruening, *J. Am. Chem. Soc.* 126 (2004) 2658-2659.
- [11] X. Xu, Y. Li, Y. Gong, P. Zhang, H. Li, Y. Wang, *J. Am. Chem. Soc.* 134 (2012) 16987-16990.
- [12] P. Zhang, Y. Gong, H. Li, Z. Chen, Y. Wang, *Nat. Commun.* 4 (2013) 1593.
- [13] Z. Wei, Y. Gong, T. Xiong, P. Zhang, H. Li, Y. Wang, *Catal. Sci. Technol.* 5 (2015) 397-404.
- [14] K. Szőri, R. Puskás, G. Szöllősi, I. Bertóti, J. Szépvölgyi, M. Bartók, *Catal. Lett.* 143 (2013) 539-546.
- [15] A.M. Raspolli Galletti, L. Toniolo, C. Antonetti, C. Evangelisti, C. Forte, *Appl. Catal. A Gen.* 447-448 (2012) 49-59.
- [16] T.-Y. Zeng, Z.-M. Zhou, J. Zhu, Z.-M. Cheng, P.-Q. Yuan, W.-K. Yuan, *Catal. Today* 147, Supplement (2009) S41-S45.
- [17] P. Serp, E. Castillejos, *ChemCatChem* 2 (2010) 41-47.
- [18] S.-Y. Ding, J. Gao, Q. Wang, Y. Zhang, W.-G. Song, C.-Y. Su, W. Wang, *J. Am. Chem. Soc.* 133 (2011) 19816-19822.
- [19] S. Mandal, D. Roy, R.V. Chaudhari, M. Sastry, *Chem. Mater.* 16 (2004) 3714-3724.
- [20] D. De Vos, I.F. Vankelecom, P.A. Jacobs, John Wiley & Sons 2008.
- [21] R. Nie, J. Shi, W. Du, Z. Hou, *Appl. Catal. A Gen.* 473 (2014) 1-6.
- [22] P. Lu, C.T. Campbell, Y. Xia, *Nano Lett.* 13 (2013) 4957-4962.
- [23] B.K. Vu, M.B. Song, I.Y. Ahn, Y.-W. Suh, D.J. Suh, W.-I. Kim, H.-L. Koh, Y.G. Choi, E.W. Shin, *Catal. Today* 164 (2011) 214-220.
- [24] R. Kou, Y. Shao, D. Mei, Z. Nie, D. Wang, C. Wang, V.V. Viswanathan, S. Park, I.A. Aksay, Y. Lin, Y. Wang, J. Liu, *J. Am. Chem. Soc.* 133 (2011) 2541-2547.

- [25] X. Wang, G. Sun, P. Routh, D.-H. Kim, W. Huang, P. Chen, *Chem. Soc. Rev.* 43 (2014) 7067-7098.
- [26] R. Nie, J. Shi, W. Du, W. Ning, Z. Hou, F.-S. Xiao, *J. Mater. Chem. A* 1 (2013) 9037-9045.
- [27] G. Vilé, D. Albani, M. Nachtegaal, Z. Chen, D. Dontsova, M. Antonietti, N. López, J. Pérez-Ramírez, *Angew. Chem. Int. Ed.* 54 (2015) 11265-11269.
- [28] E. Haque, J.W. Jun, S.N. Talapaneni, A. Vinu, S.H. Jung, *J. Mater. Chem.* 20 (2010) 10801-10803.
- [29] Y. Gao, G. Hu, J. Zhong, Z. Shi, Y. Zhu, D.S. Su, J. Wang, X. Bao, D. Ma, *Angew. Chem. Int. Ed.* 52 (2013) 2109-2113.
- [30] Z. Wei, J. Wang, S. Mao, D. Su, H. Jin, Y. Wang, F. Xu, H. Li, Y. Wang, *ACS Catal.* 5 (2015) 4783-4789.
- [31] D. He, Y. Jiang, H. Lv, M. Pan, S. Mu, *Appl. Catal. B Environ.* 132-133 (2013) 379-388.
- [32] L. Jia, D.A. Bulushev, O.Y. Podyacheva, A.I. Boronin, L.S. Kibis, E.Y. Gerasimov, S. Beloshapkin, I.A. Seryak, Z.R. Ismagilov, J.R.H. Ross, *J. Catal.* 307 (2013) 94-102.
- [33] R. Arrigo, M.E. Schuster, S. Wrabetz, F. Girgsdies, J.-P. Tessonnier, G. Centi, S. Perathoner, D.S. Su, R. Schlögl, *ChemSusChem* 5 (2012) 577-586.
- [34] R. Arrigo, M.E. Schuster, Z. Xie, Y. Yi, G. Wowsnick, L.L. Sun, K.E. Hermann, M. Friedrich, P. Kast, M. Hävecker, A. Knop-Gericke, R. Schlögl, *ACS Catal.* 5 (2015) 2740-2753.
- [35] R. Arrigo, M.E. Schuster, S. Abate, S. Wrabetz, K. Amakawa, D. Teschner, M. Freni, G. Centi, S. Perathoner, M. Hävecker, *ChemSusChem* 7 (2014) 179-194.
- [36] X. Xu, M. Tang, M. Li, H. Li, Y. Wang, *ACS Catal.* 4 (2014) 3132-3135.
- [37] H.-W. Lin, C.H. Yen, C.-S. Tan, *Green Chem.* 14 (2012) 682-687.
- [38] M. Tang, S. Mao, M. Li, Z. Wei, F. Xu, H. Li, Y. Wang, *ACS Catal.* 5 (2015) 3100-3107.
- [39] J.M. Thomas, B.F. Johnson, R. Raja, G. Sankar, P.A. Midgley, *Acc. Chem. Res.* 36 (2003) 20-30.

- [40] X. Wen, Y. Cao, X. Qiao, L. Niu, L. Huo, G. Bai, *Catal. Sci. Technol.* 5 (2015) 3281-3287.
- [41] G. Bai, X. Wen, Z. Zhao, F. Li, H. Dong, M. Qiu, *Ind. Eng. Chem. Res.* 52 (2013) 2266-2272.
- [42] R.L. Augustine, *Catal. Rev. Sci. Eng.* 13 (1976) 285-316.
- [43] Z. Duan, Z. Wang, C. Sun, L. Zhao, Y. Wang, *RSC Adv.* 5 (2015) 56808-56814.
- [44] A. Vinu, *Adv. Funct. Mater.* 18 (2008) 816-827.
- [45] R. Nie, J. Wang, L. Wang, Y. Qin, P. Chen, Z. Hou, *Carbon* 50 (2012) 586-596.
- [46] G.P. Mane, S.N. Talapaneni, C. Anand, S. Varghese, H. Iwai, Q. Ji, K. Ariga, T. Mori, A. Vinu, *Adv. Funct. Mater.* 22 (2012) 3596-3604.
- [47] K. Parvez, S. Yang, Y. Hernandez, A. Winter, A. Turchanin, X. Feng, K. Müllen, *ACS Nano* 6 (2012) 9541-9550.
- [48] J. Xu, T. Chen, Q. Jiang, Y.-X. Li, *Chem. Asian J.* 9 (2014) 3269-3277.
- [49] A. Thomas, A. Fischer, F. Goettmann, M. Antonietti, J.-O. Müller, R. Schlögl, J.M. Carlsson, *J. Mater. Chem.* 18 (2008) 4893-4908.
- [50] X. Ning, H. Yu, F. Peng, H. Wang, *J. Catal.* 325 (2015) 136-144.
- [51] Y. Yan, Y. Dai, S. Wang, X. Jia, H. Yu, Y. Yang, *Appl. Catal. B Environ.* 184 (2016) 104-118.
- [52] Y. Yan, Y. Chen, X. Jia, Y. Yang, *Appl. Catal. B Environ.* 156-157 (2014) 385-397.
- [53] C.-S. Tsao, Y.-R. Tzeng, M.-S. Yu, C.-Y. Wang, H.-H. Tseng, T.-Y. Chung, H.-C. Wu, T. Yamamoto, K. Kaneko, S.-H. Chen, *J. Phy. Chem. Lett.* 1 (2010) 1060-1063.
- [54] Y. Zhou, K. Neyerlin, T.S. Olson, S. Pylypenko, J. Bult, H.N. Dinh, T. Gennett, Z. Shao, R. O'Hayre, *Energy Environ. Sci.* 3 (2010) 1437-1446.
- [55] L. Bulusheva, A. Okotrub, A. Kurennya, H. Zhang, H. Zhang, X. Chen, H. Song, *Carbon* 49 (2011) 4013-4023.
- [56] Y.-H. Li, T.-H. Hung, C.-W. Chen, *Carbon* 47(2009) 850-855.
- [57] T. He, L. Liu, G. Wu, P. Chen, *J. Mater. Chem. A* 3 (2015) 16235-16241.

- [58] R. Nie, H. Jiang, X. Lu, D. Zhou, Q. Xia, *Catal. Sci. Technol.* 6 (2016) 1913-
DOI: 10.1039/C5CY01418B.
- [59] Y. Wang, J. Yao, H. Li, D. Su, M. Antonietti, *J. Am. Chem. Soc.* 133 (2011)
2362-2365.
- [60] N. Mahata, K. Raghavan, V. Vishwanathan, C. Park, M. Keane, *Phys. Chem.
Chem. Phys.* 3 (2001) 2712-2719.
- [61] G. Neri, A. Visco, A. Donato, C. Milone, M. Malentacchi, G. Gubitosa, *Appl.
Catal. A Gen.* 110 (1994) 49-59.
- [62] H. Li, J. Liu, S. Xie, M. Qiao, W. Dai, Y. Lu, H. Li, *Adv. Funct. Mater.* 18
(2008) 3235-3241.

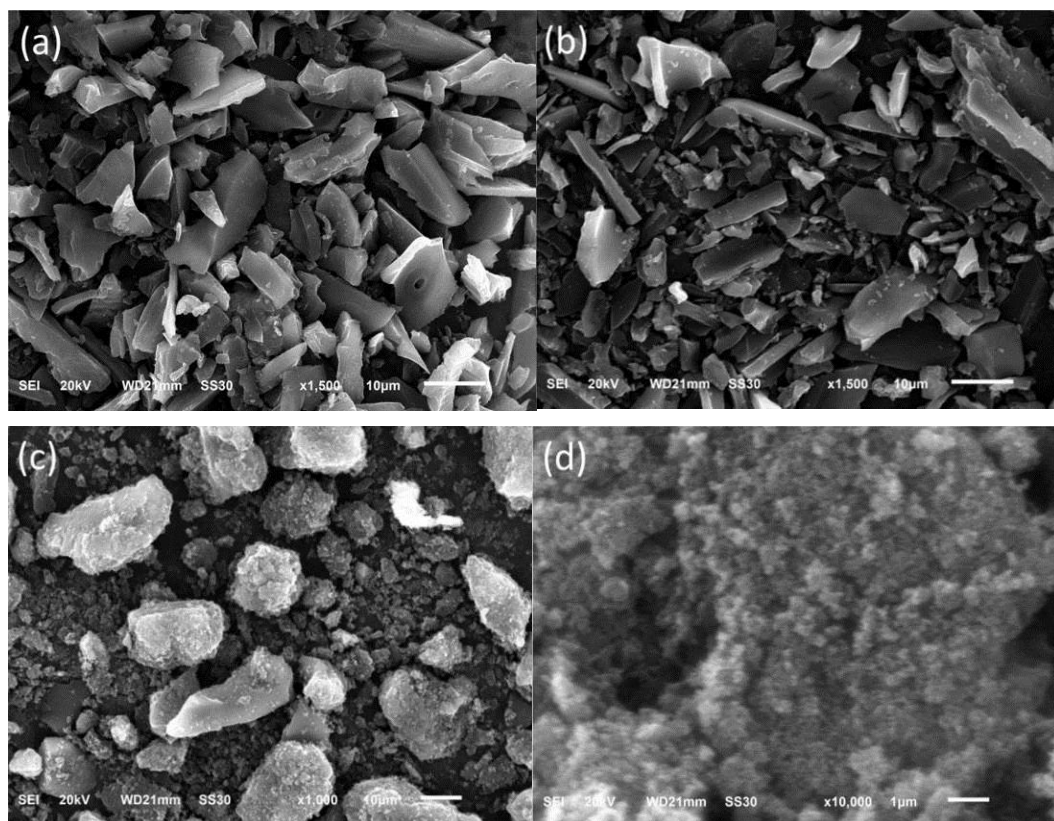


Fig. 1. SEM images of (a) AC, (b) NAC and (c,d) MCN.

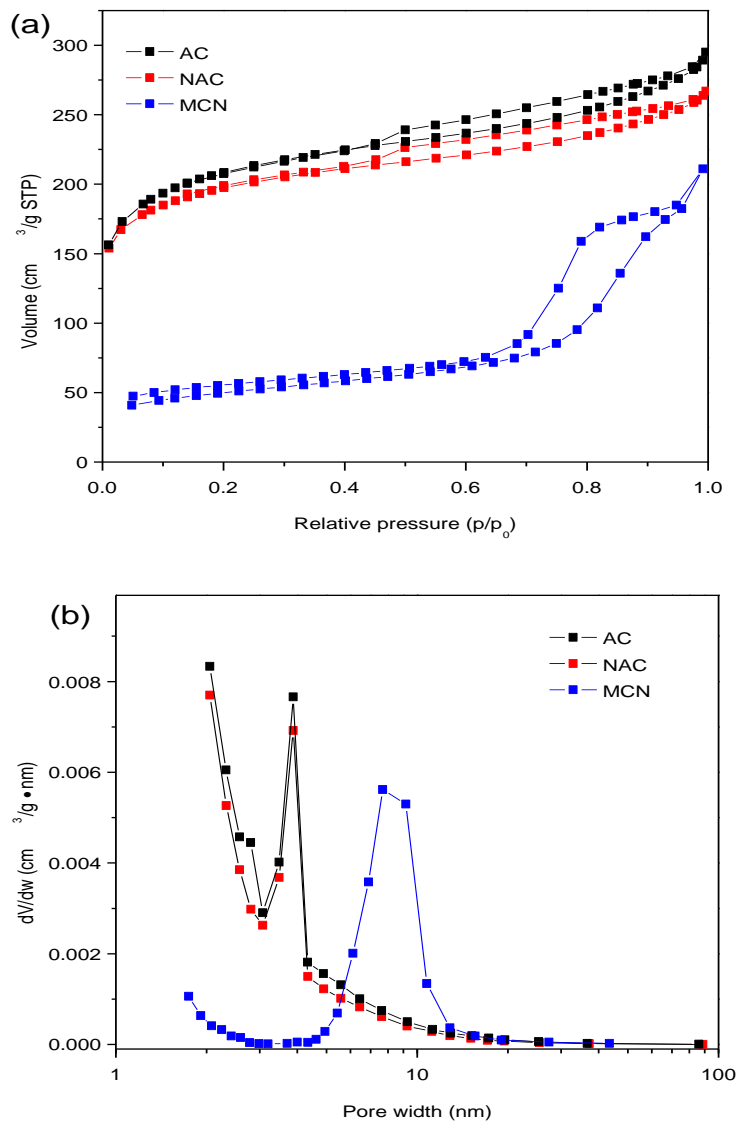


Fig. 2. (a) Nitrogen sorption isotherms and (b) pore size distribution of the samples.

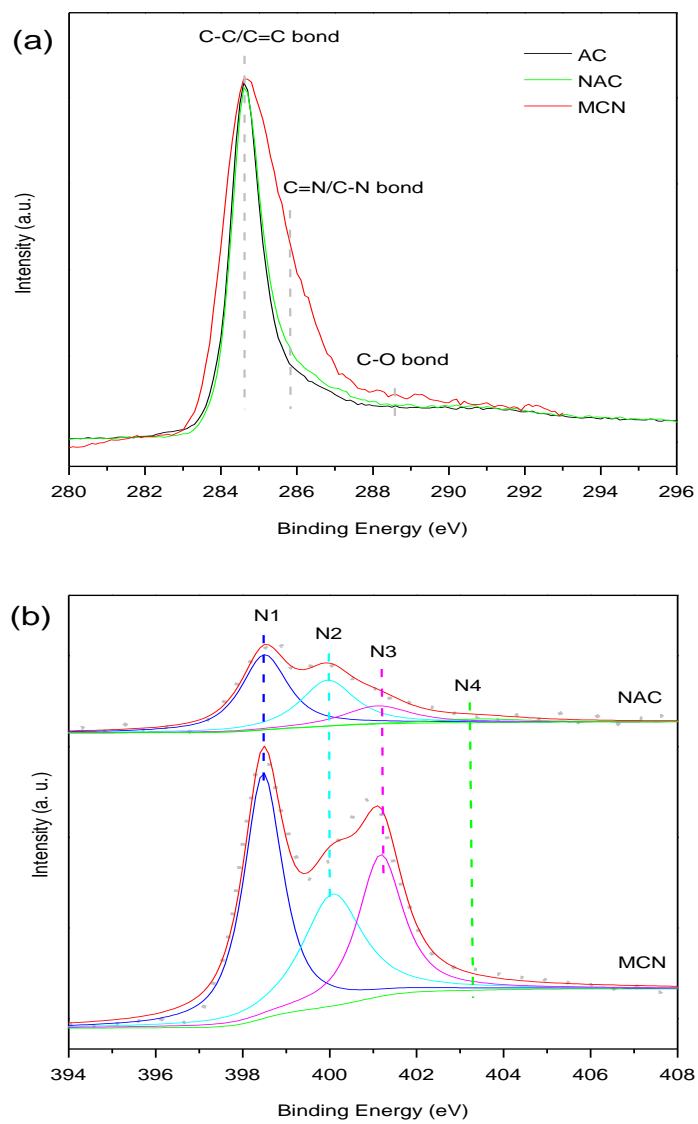


Fig. 3. XPS spectra of (a) C1s and (b) N1s in the samples.

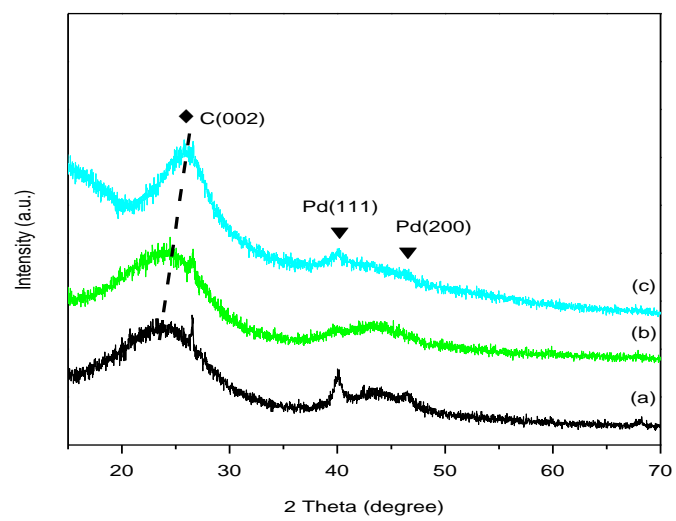
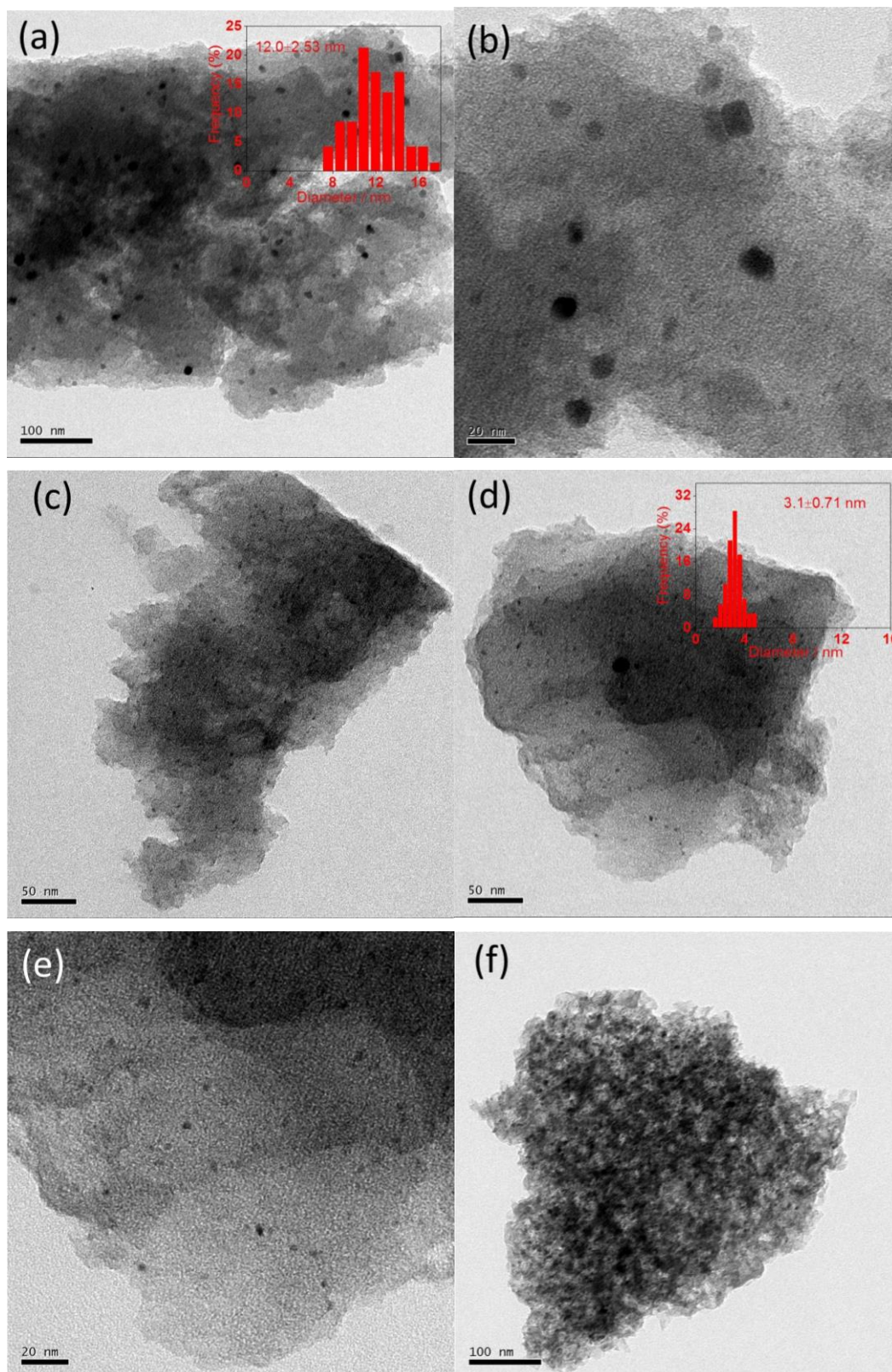


Fig. 4. XRD patterns of (a) Pd/AC, (b) Pd/NAC and (c) Pd/MCN.



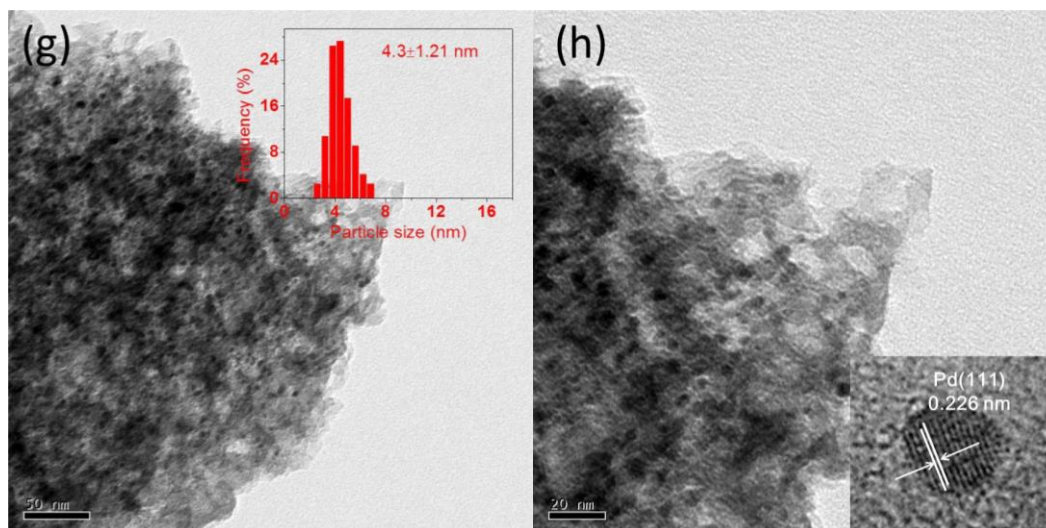


Fig. 5. TEM images of (a, b) Pd/AC, (c-e) Pd/NAC and (f-h) Pd/MCN. The insets in images of (a, d and g) corresponding to histograms of Pd particle size distribution. The inset in image of (h) is high resolution TEM image of Pd nanoparticles in Pd/MCN.

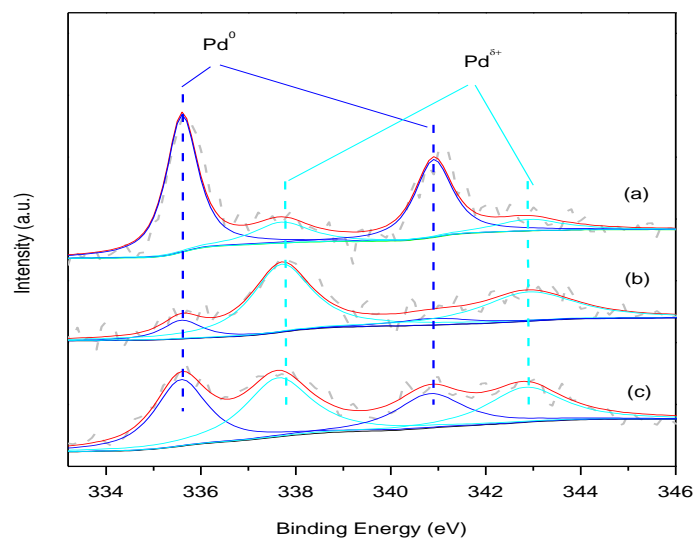


Fig. 6. Pd3d spectra of (a) Pd/AC, (b) Pd/NAC and (c) Pd/MCN.

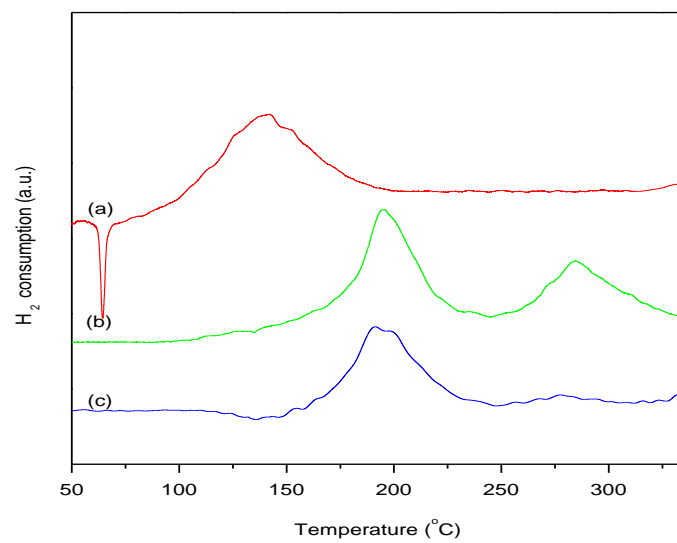


Fig. 7. H₂-TPR curves of (a) Pd/AC, (b) Pd/NAC and (c) Pd/MCN.

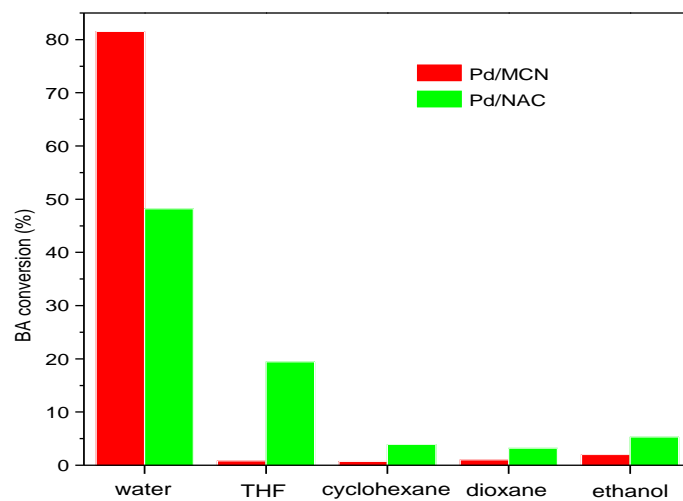


Fig. 8. Hydrogenation of BA in different solvents over Pd/MCN and Pd/NAC.

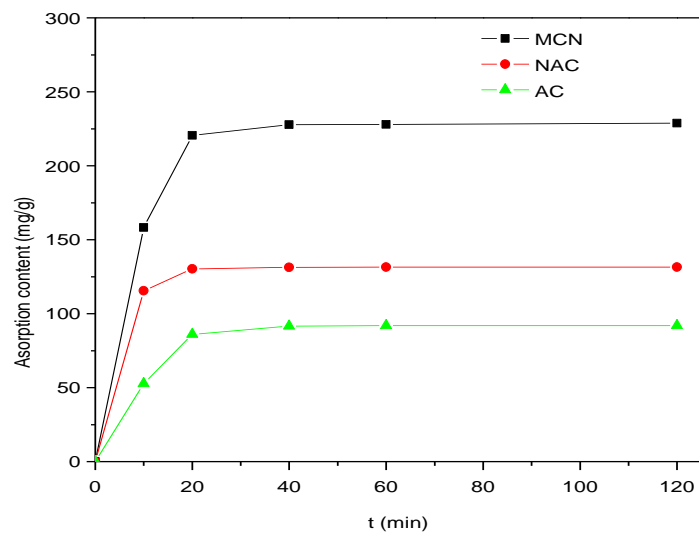


Fig. 9. Adsorption kinetics of BA over AC, NAC and MCN supports.

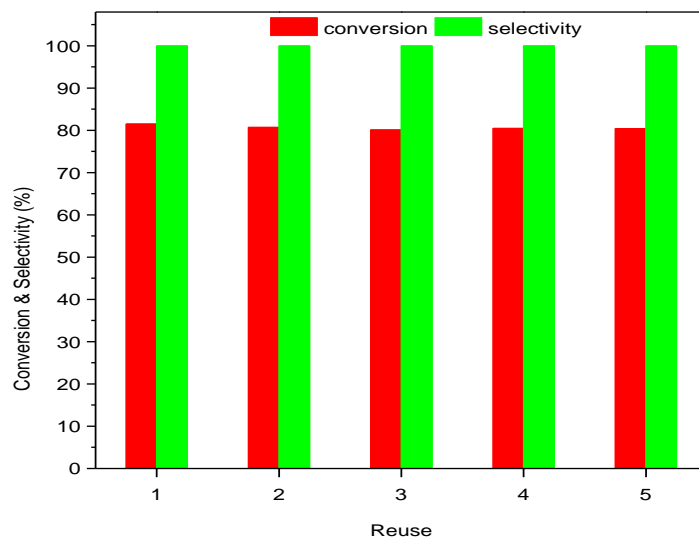


Fig. 10. Re-uses of Pd/MCN for BA hydrogenation.

Reaction conditions: 0.5 mmol BA, catalyst 20 mg, 5 mL H₂O, 2.5 MPa H₂, 110 °C, 2h.

Table 1. Structural properties of the samples.

Samples	S_{total} (m^2g^{-1})	Surface area (m^2/g)			$V_{\text{meso}}/$ V_{total} (%)	Average pore diameter (nm)	ζ Potential (mV)
		V_{total} (cm^3/g)	V_{micro} (cm^3/g)	V_{meso} (cm^3/g)			
AC	718.5	0.44	0.24	0.20	45.5	4.3	-0.02
NAC	677.2	0.40	0.24	0.16	40.0	4.1	-17.0
MCN	166.3	0.33	0.06	0.27	81.8	9.2	-25.4

Table 2. Chemical compositions of N-doped carbon catalysts.^a

Catalysts	Mass concentration (%)					
	C	O	N	N ^b	Pd	Pd ^c
Pd/AC	89.05	8.50	-	-	2.45	2.31
Pd/NAC	85.89	7.93	3.76	2.35	2.42	2.33
Pd/MCN	71.55	7.59	18.45	18.34	2.41	2.39

^a Mass concentrations were detected in XPS analysis.

^b Detected by CHNS elemental analysis, the value was the relative quantity to the mass of C.

^c Detected *via* ICP, the value was the relative quantity to the mass of C.

Table 3. Structural parameters of Pd-based catalysts.

Catalysts	Particle size (nm)		Relative atomic percentage (%)				Relative atomic percentage (%)	
	XRD	TEM	N1	N2	N3	N4	Pd ⁰	Pd ^{δ+}
Pd/AC	10.8	12.0	-	-	-		78.6	21.4
Pd/NAC	2.4	3.1	51.4	39.8	8.7	0.1	15.5	84.5
Pd/MCN	3.8	4.3	40.2	26.3	31.7	1.8	46.1	53.9

Table 4. Hydrogenation of BA over different catalysts.^a

Entry	Catalysts	t (h)	T (°C)	Conversion (%)	Selectivity (%)
1	No catalyst	2	110	<0.1	-
2	Pd/AC	2	110	7.2	100
3	Pd/NAC	2	110	48.2	100
4	Pd/MCN	2	110	81.5	100
5	Pd/MCN	2.5	110	100	100
6	Pd/AC ^b	2	110	24.5	100
7	Pd/SiO ₂	2	110	1.2	100
8	Pd/Al ₂ O ₃	2	110	0.4	100
9	Pd/MgO	2	110	5.6	100

^a Reaction conditions: 0.5 mmol BA, catalyst 20 mg, 5 mL H₂O, 2.5 MPa H₂.

^b Purchased from Aladdin company.

Table 5. Hydrogenation of benzamide over different catalysts.^a

Entry	Catalysts	t (h)	T (°C)	Conversion (%)	Selectivity (%)
1	Pd/AC	8	85	4.4	100
2	Pd/NAC	8	85	15.5	100
3	Pd/MCN	8	85	55.6	100
4	Pd/MCN	4	110	100	91

^a Reaction conditions: 0.5 mmol benzamide, catalyst 20 mg, 5 mL H₂O, 2.5 MPa H₂.

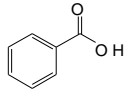
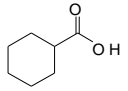
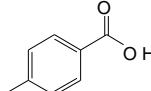
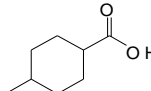
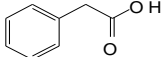
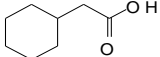
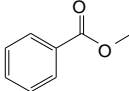
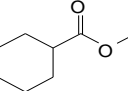
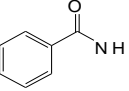
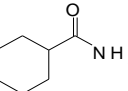
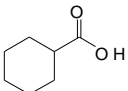
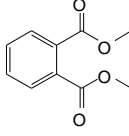
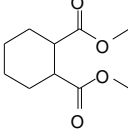
Table 6. Hydrogenation of phenol over different catalysts.^a

Entry	Catalysts	t (h)	T (°C)	Conversion (%)	Selectivity (%)
1	Pd/AC	4	40	24.8	93.5
2	Pd/NAC	4	40	53.7	95.1
4	Pd/MCN	4	40	100	98.1

^a Reaction conditions: 19.6 mg (0.2 mmol) phenol, 20 mg catalyst, 5 mL H₂O, 40 °C, 0.3 MPa H₂

o

Table 7. Hydrogenation of benzoic acid derivatives over Pd/MCN catalyst.^a

Entry	Substrate	Product	T (h)	T (°C)	Conversion (%)	Selectivity (%)
1			2.5	110	100	100
2			2	110	98	100 trans:cis = 67:33
3			4	110	100	100
4			6	110	100	100
5		 	4	110	100	91 9
6			8	110	92	100 trans:cis = 5:95

^a Reaction conditions: 0.5 mmol substrate, 20 mg catalyst, 5 mL H₂O, 2.5 MPa H₂.